*remote sensing*

MDPI

*Article*

# Simulating the Net Primary Production of Even-Aged Forests by the Use of Remote Sensing and Ecosystem Modelling Techniques

**Marta Chiesi [1], Luca Fibbi [1,2,*], Silvana Vanucci [3], Lorenzo Bottai [2], Gherardo Chirici [4] and Fabio Maselli [1]**

[1] CNR IBE, 50019 Sesto Fiorentino, Italy; marta.chiesi@cnr.it (M.C.); fabio.maselli@cnr.it (F.M.)
[2] LaMMA Consortium, 50019 Sesto Fiorentino, Italy; bottai@lamma.toscana.it
[3] Department of Chemical, Biological, Pharmaceutical and Environmental Sciences (ChiBioFarAm), University of Messina, 98166 Messina, Italy; silvana.vanucci@unime.it
[4] Department of Agriculture, Food, Environment and Forestry (DAGRI), University of Florence, 50145 Florence, Italy; gherardo.chirici@unifi.it
* Correspondence: luca.fibbi@cnr.it

**Abstract:** A recently proposed modelling strategy predicts the net primary production (NPP) of forest ecosystems by combining the outputs of a NDVI-driven model, Modified C-Fix, and a biogeochemical model, BIOME-BGC. This combination strategy takes into account the effects of forest disturbances but still assumes the presence of a mixture of differently aged trees. The application of this strategy to even-aged forests, therefore, requires a methodological advancement aimed at properly modifying the modelling of main ecosystem processes. In particular, the adaptation of the method to even-aged forests is based on the use of high-spatial-resolution airborne laser scanning (ALS) datasets, which yields green and woody biomass estimates that regulate the simulation of photosynthetic and respiratory processes, respectively. This approach was experimented in a Mediterranean study area, San Rossore Regional Park (Central Italy), which is covered by even-aged pine stands in different development phases. The modelling strategy is driven by MODIS NDVI images and meteorological data across five years (2011–2015), which are combined with estimates of forest canopy cover and height obtained from ALS data taken in 2015. This allows the production of stand NPP estimates, which, when converted into respective current annual increment (CAI) values, reasonably reproduce the age dependency of the available ground observations. The CAI estimates also show a highly significant correlation with these observations (r = 0.773) and moderate error levels (RMSE = 2.03 $m^3$ $ha^{-1}$ $year^{-1}$, MBE = −0.45 $m^3$ $ha^{-1}$ $year^{-1}$). These results confirm the potential of the modified simulation method to yield accurate high-spatial-resolution NPP estimates, which can offer valuable insights into C cycling and storage, in even-aged forests.

**Keywords:** Mediterranean forest; MODIS NDVI; C-Fix; ALS data; CAI



**Citation:** Chiesi, M.; Fibbi, L.; Vanucci, S.; Bottai, L.; Chirici, G.; Maselli, F. Simulating the Net Primary Production of Even-Aged Forests by the Use of Remote Sensing and Ecosystem Modelling Techniques. *Remote Sens.* **2024**, *16*, 2155. https://doi.org/10.3390/rs16122155

Academic Editor: Henning Buddenbaum

Received: 11 April 2024
Revised: 6 June 2024
Accepted: 11 June 2024
Published: 14 June 2024



## 1. Introduction

Forest ecosystems, which are distributed over almost one-third of terrestrial, ice-free surfaces, play a significant role in the global carbon (C) cycle due to their capacity to store carbon within their tissues [1,2]. Recently, large discussions have emerged about the possibility of investing in reforestation and/or forest regeneration to mitigate the effects of climate change [3,4]; this has stimulated the scientific community to investigate the quantification of forest ecosystem production. Quantifying the role of forests is particularly important in regions for which there are large uncertainties in the carbon balance, such as those surrounding the Mediterranean basin. In fact, in these regions, forest ecosystems have been considered both as weak sources and as sinks, with most uncertainties induced by the long disturbance history and the more recent impact of climate change [5].

The accumulation of new biomass within forest ecosystems is usually quantified as net primary production (NPP), which corresponds to the difference between photosynthesis and autotrophic respiration [6,7]. This variable is generally assessed by means of national

forest inventories [8] and, more specifically, via the estimation of the current annual increment (CAI), which is convertible into dry matter (or carbon) NPP through the use of species-specific biomass expansion factors (BEFs) [9,10]. The methods applied to retrieve NPP and CAI based on field data, however, are more complex, time- and cost-consuming, and affected by possible errors than those applied to assess basic forest attributes (e.g., tree density and height, basal area, stem volume, etc.) [11–13].

Remote sensing techniques and biogeochemical models can be used as alternative tools to study and monitor the main forest ecosystem processes. The former, in fact, can directly estimate spatially and temporally variable vegetation features, while the latter can simulate all main vegetation processes (e.g., photosynthesis, respiration, and allocations). Therefore, these two techniques are intrinsically complementary and can be suitably combined for simulating forest C fluxes, particularly NPP [14–17]. Maselli et al. [18], for example, proposed to combine the outputs of a radiation use efficiency (RUE) model, Modified C-Fix, with those of a model of ecosystem processes, BIOME-BGC. The former model estimates forest gross primary production (GPP) based on standard meteorological observations and remotely sensed NDVI images, while the latter simulates all main ecosystem processes driven only by ancillary data descriptive of forest conditions. The outcomes of the two models are finally combined using the ecosystem equilibrium theory to take into account the effects of forest disturbances [18]. More specifically, the equilibrium condition simulated by BIOME-BGC is converted into the condition of real ecosystems through the use of a proxy variable of woody biomass given by the ratio of actual over potential growing stock volume (GSV).

This modelling strategy relies on the assumption that the examined ecosystems are composed of a mixture of trees in heterogeneous development stages, which mimics the structure and functions of forests simulated via BIOME-BGC. Hence, the application of the strategy to even-aged forest stands, where this condition is not met, implies an additional issue. In these cases, in fact, the relationship between forest green and woody biomass pools can be profoundly altered depending on the stand structure and development phase, which induce relevant modifications of photosynthetic and respiratory processes [19–21]. This issue, which usually determines a decrease in the green/woody biomass ratio during stand development, was addressed by [22], who introduced an age-dependent correction aimed at modifying the simulation of tree photosynthesis and autotrophic respiration. This operation required a local calibration of the method based on ground observations of tree growth increments, which is obviously impractical for operational forest monitoring programmes over large areas.

A more recent study has postulated that a similar correction can be obtained by the processing of high-spatial-resolution airborne laser scanning (ALS) observations, which are now widely available [23]. ALS data, in fact, are informative in terms of the green and woody biomass pools existing in each ecosystem, which are the main regulators of photosynthetic and respiratory processes, respectively. Therefore, the accurate quantification of such pools is expected to improve the capacity of the original modelling strategy to reproduce these processes, particularly concerning their age dependency. This should allow an enhanced simulation of the C stored in managed forests, which is fundamental for both scientific and practical reasons.

This expectation can be investigated using a set of ground and remotely sensed datasets descriptive of even-aged forest stands that include observations of CAI as a proxy of NPP. This study pursues this objective by relying on a dataset collected in the pine wood of the San Rossore Regional Park (Central Italy), which has been the subject of numerous previous research activities and forest surveys (e.g., [24]). More specifically, the investigation is aimed at evaluating the improvement that can be obtained by feeding the original NPP modelling strategy with ALS estimates of the existing green and woody biomass pools, which vary depending on the age of the stand.

## 2. Materials and Methods

### *2.1. Study Area*

The San Rossore Regional Park, which has been the subject of several investigations concerning all main forest processes (e.g., [18,22,23]), is located in a flat coastal area close to Pisa, Central Italy (43.68–43.78°N Lat., 10.27–10.35°E Long.; Figure 1). The climate of the area is Mediterranean, with a mean annual temperature around 15 °C and a mean annual rainfall about 900 mm; precipitation shows a minimum in summer and two maxima in spring and autumn, which induces a clear summer dry period. The area has prevalently deep, sandy soils, sometimes affected by problems of salinity.

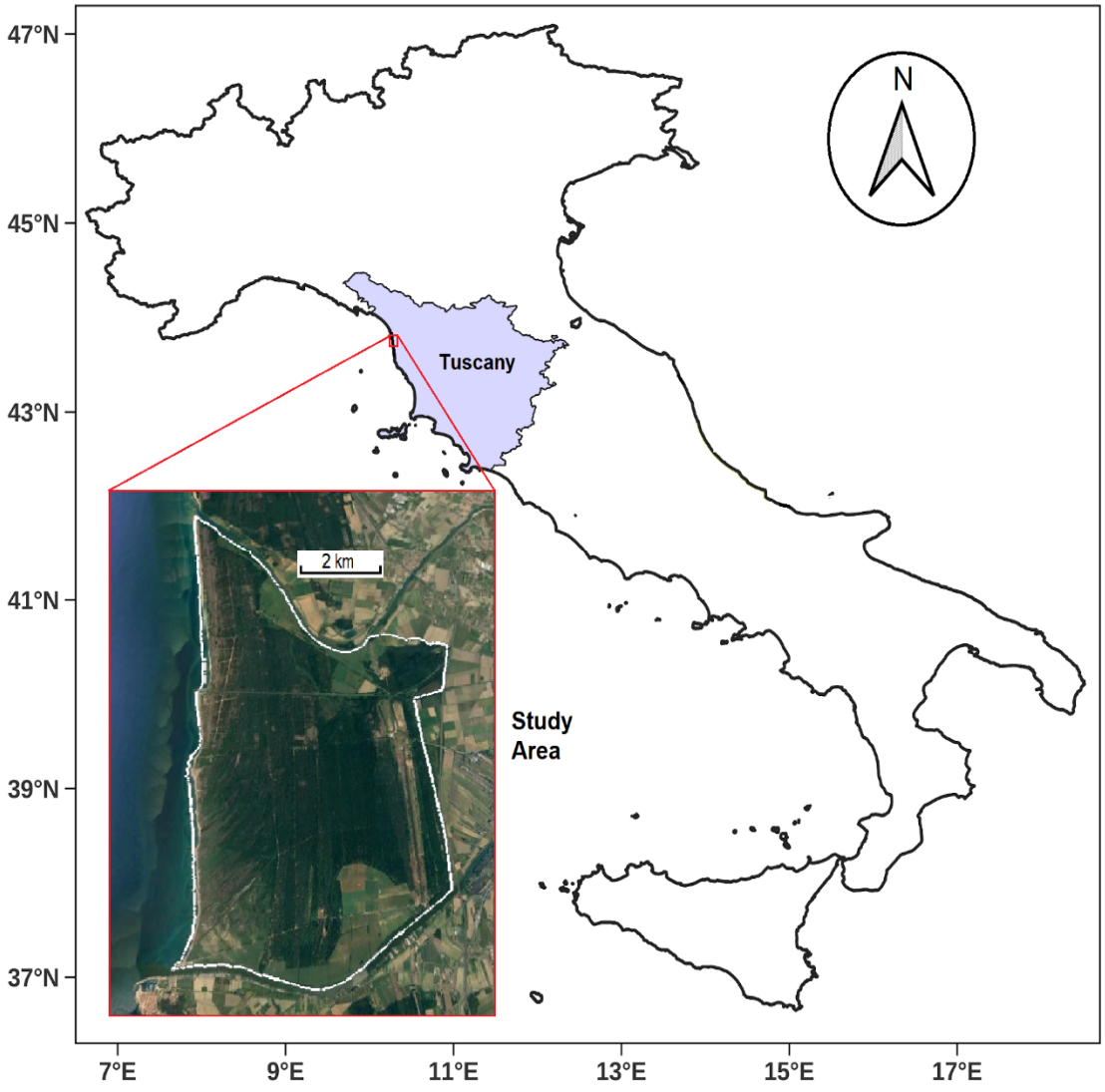


**Figure 1.** Geographical position of the study area in Italy and, enlarged, Google Earth image taken in August 2015, showing the San Rossore Park bounded by the white line.

The park includes a coastal strip dominated by a *Pinus pinea* L. (umbrella pine) forest, which is predominantly in an old growth phase. Most even-aged *P. pinea* stands are, in fact, over 50 years old, relatively dense and have a mean height of 20–22 m; only a few of them are younger (trees planted about 30 years ago) and have a height of 15–18 m.

### *2.2. Study Data*

A description of most pine forest stands in the park was provided in the framework of the San Rossore Forest Inventory (SRFI), which referred to the years around 2000 [25].

This inventory reports the number of trees per hectare, the mean canopy height (CH, m), the diameter at breast height (DBH, cm), the basal area (BA, $m^2$ $ha^{-1}$), the GSV ($m^3$ $ha^{-1}$), and the CAI ($m^3$ $ha^{-1}$ $y^{-1}$) of some stands, which were utilized in the current work. The same forest attributes were measured during another forest inventory repeated after about 20 years; the stand observations of this inventory have been obtained via personal contact with the park administration.

Spatially interpolated daily estimates of minimum and maximum air temperature and rainfall for five years (2011–2015) were derived from the ground observations of the LaMMA Consortium (http://www.lamma.toscana.it/, accessed on 8 January 2024) [26]. Solar radiation was then estimated by means of the ERAD algorithm proposed by [27], which is based on Meteosat Second Generation satellite data. All these datasets have a spatial resolution consistent with that of MODIS NDVI imagery, i.e., about 250 m.

Normalized difference vegetation index (NDVI) images taken using the Moderate Resolution Imaging Spectroradiometer (MODIS) were derived from the NASA archive (https://modis.gsfc.nasa.gov, accessed on 8 January 2024). This product provided maximum value composite (MVC) images referring to 16-day periods and it has a spatial resolution of 250 m. All MVC images of the study area over the same years as above (2011–2015) were further pre-processed in order to reduce residual atmospheric contamination (for details, see [18,28]).

This study also considered a high-spatial-resolution ALS acquisition taken over the San Rossore Park during helicopter flights performed between 5th and 8th May 2015. The helicopter operated at an altitude of about 1100 m a.s.l. with a speed of 70 kn and acquired data with a maximum scan angle of 60°, resulting in a mean SWAT of 1100 m. The helicopter was equipped with a LiDAR RIEGL LMS-Q680i system, which emitted 4.4 pulses $m^{-2}$ in a full waveform modality and acquired at a wavelength of 1550 nm; the pulse frequency was 300 kHz, with 80 lines per second and 2500 measurements per line. The original data were processed to yield 1 m spatial resolution digital surface and terrain models of the area, from which the canopy height model (CHM) of the vegetated land surfaces was obtained.

### *2.3. NPP Modelling Strategy*

The main characteristics of the two models applied (Modified C-Fix and BIOME-BGC), and the combination of their outputs are summarized in the following paragraphs; additional details, together with relevant assumptions and approximations, can be found in [18] and [28]. C-Fix is a RUE model driven by daily meteorological and NDVI data, which was modified by [29] to improve GPP prediction in Mediterranean water-limited environments. In fact, Modified C-Fix includes a water stress scalar (Cws) obtained from meteorological data, which simulates the impact of short-term water stress on forest GPP. Hence, the model estimates the GPP of day i ($GPP_i$) as follows:

$$GPP_i = \varepsilon \cdot Tcor_i \cdot Cws_i \cdot fAPAR_i \cdot PAR_i \quad (1)$$

where $\varepsilon$ is the maximum RUE of forests (1.2 g C $MJ^{-1}$ APAR), $Tcor_i$ is the respective temperature correction scalar based on minimum temperature [30], $fAPAR_i$ is the fraction of absorbed photosynthetically active radiation (PAR) derived from NDVI, and $PAR_i$ is the incident PAR derived as a constant fraction of solar radiation, which all refer to day i. The water stress scalar of each day ($Cws_i$), which ranges from 0.5 to 1, is derived from the ratio between rainfall and potential evapotranspiration (PET), both cumulated over the preceding two months.

BIOME-BGC is a bio-geochemical model that predicts the storage and fluxes of water, C and nitrogen in terrestrial ecosystems [31]. This model can simulate all pools and processes of ecosystems in a quasi-equilibrium condition using daily meteorological data and site information on soil, vegetation, and eco-physiological parameters [32]. BIOME-BGC then proceeds with a normal simulation of photosynthesis, respiration, and allocation processes referring to the examined study period. The quasi-equilibrium simulation implies that the annual sum of all respirations roughly equals GPP, while the mean annual NEP

tends toward zero. The parameter settings originally provided with version (4.2) of the used model for seven biome types were modified to suit Mediterranean water-stressed conditions (e.g., [28]).

The RUE model offers the advantage of a direct remote sensing estimation of total forest GPP, while BIOME-BGC allows for a complete simulation of all main ecosystem processes. Therefore, the estimates of the latter model can be improved via the multiplication of the ratio between C-Fix and BIOME-BGC GPP [18]. The outputs obtained must also be corrected for the effects exerted by natural and/or human-induced disturbances on actual forest conditions [33]. Such disturbances tend to reduce the biomass pools of forest ecosystems and subsequently induce positive NEP due to new C accumulation. Following this reasoning, the ratio of actual over potential GSV is assumed to represent the distance from ecosystem equilibrium, and it is used to correct the estimated C fluxes. Thus, the actual forest NPP of day i ($NPP_i$) is estimated as follows:

$$NPP_i = GPP_i \cdot FC - Rgr_i \cdot FC - Rmn_i \cdot NV \quad (2)$$

where $GPP_i$, $Rgr_i$, and $Rmn_i$ are the BIOME-BGC estimates of photosynthesis, growth, and maintenance respirations improved by the combination with C-Fix GPP, while the two scalars FC (fractional forest cover) and NV (normalized GSV) describe the ecosystem distance from the equilibrium condition [18,24]. In particular, FC regulates the forest processes related to tree photosynthesis, while NV affects maintenance respiration. Forest NPP is, therefore, dependent on the relationship between the two scalars, which were originally both derived from the ratio of actual over potential GSV [18]. Distinctively, FC was obtained by applying Beers's law to the actual leaf area index (LAI), which was calculated as the product of NV and maximum forest LAI simulated by BIOME-BGC. This method, however, is effective only in semi-natural forest ecosystems composed of differently aged trees, where the green and woody biomass pools are approximately in equilibrium, as assumed when using BIOME-BGC.

The case is different for even-aged stands, in which the ratio between these pools can strongly differ from that simulated when using the model. In fact, in these stands, the green biomass rapidly reaches near-maximum values, while the woody biomass continues to increase, depending also on the management practices applied. Consequently, the ratio between the two biomass pools tends to decrease with stand aging, which has notable consequences on the balance between photosynthetic and respiratory processes [34]. In a preliminary study, [23] hypothesized that this issue can be addressed by estimating both FC and NV via the processing of high-spatial-resolution ALS data. These data are, in fact, intrinsically capable of providing information on the actual structure of forest ecosystems, particularly tree leafage and GSV [35]. The independent estimation of existing green and woody biomass pools is expected to allow for a more flexible and efficient simulation of the stand photosynthetic and respiratory processes and, consequently, NPP.

The effects of estimating the two scalars of Equation (2) following the original and this new method are illustrated in Figure 2. Deriving FC from NV through the use of Beer's law yields a unique exponential relationship between the two scalars dependent on BIOME-BGC potential LAI. On the contrary, estimating NV and FC separately allows for the simulation of all possible relationships between the two scalars. More specifically, considering the proportionality between BA and FC found by [36], a family of linear relationships between FC and NV is obtained with null offsets and slopes inversely related to CH. This obviously affects the NPP simulated via Equation (2), which becomes dependent linearly on CH and, asymptotically, on age, due to the tendency of CH to level off with stand aging.

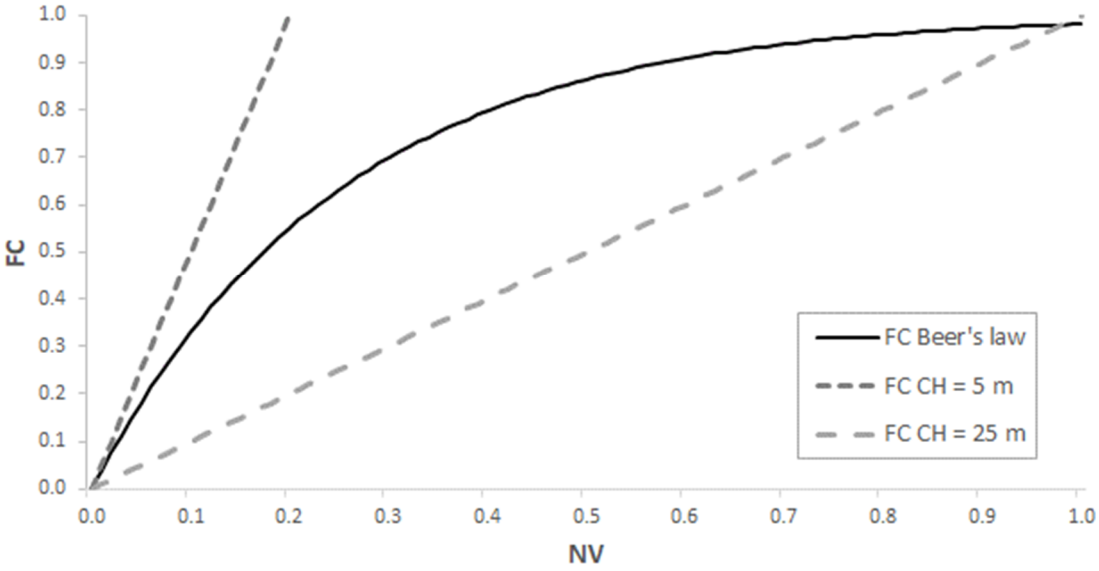


**Figure 2.** Examples of relationships between FC and NV obtained via the original and new estimation methods. The solid exponential curve shows the values of FC derived from NV through Beer's law; the two dotted lines show the same values estimated using the BA-FC allometric equation of [36] and setting CH to 5 and 25 m, which correspond to a juvenile and an old-growth stand, respectively (see text for details).

### *2.4. Data Processing*

The available ground observations of the selected umbrella pine stands derived from the two SR inventories were temporally interpolated to the year of ALS data acquisition (2015). A linear interpolation method was used for all forest attributes, with the exception of CAI, for which a reduction in the number of trees that occurred from 2000 to 2020 was taken into account. Next, both the original and modified versions of the described NPP modelling strategy were applied to all stands larger than the approximate size of a MODIS NDVI pixel (5 ha), the features of which were fully described by both inventories. Specifically, Modified C-Fix (Equations (1) and (2)) was driven by daily meteorological data of the five years preceding 2015 (2011–2015) and corresponding NDVI data extracted from the MODIS pixels that were roughly coincident with each stand. A BIOME-BGC version parameterized for Mediterranean pines was then applied using the same meteorological dataset and ancillary information [24].

The available ALS CHM was corrected as described in [36]. A height threshold (5 m) was imposed to yield stand FC estimates, which were converted into stand BA through a locally defined allometric equation [36]. Stand height was calculated as described in the same article and combined with BA to yield GSV estimates, which were normalized to NV using BIOME-BGC maximum GSV and transformed into LAI and then FC through the use of Beer' law. The outputs of the two models considered were then averaged over the study years and combined with these NV and FC estimates, as described in [36]. This method yielded stand NPP estimates, which were converted into respective CAI values through the following equation:

$$CAI = NPP \cdot SCA/BEF/BWD \cdot 2/100 \quad (3)$$

where SCA is the stem carbon allocation ratio, BEF is the volume of the above-ground biomass/standing volume biomass expansion factor (both dimensionless), and BWD is the basic wood density (Mg $m^{-3}$) [10]. The multiplication by 2 accounts for the conversion from C to dry matter, and the division by 100 accounts for the change in magnitude from g $m^{-2}$ to Mg $ha^{-1}$.

As previously noted, the application of this method considered the CAI variability derived from GSV, but yielded estimates theoretically referring to stands composed of trees in heterogeneous development stages.

The actual status of the even-aged pine wood stands was instead accounted for by modifying the model combination strategy based on the previously exposed eco-physiological considerations. This implied another application of the modelling strategy driven by the stand FC values directly obtained from ALS data in place of those derived from NV, which yielded a new set of respective NPP and CAI estimates.

The relationships between the temporally interpolated SRFI observations involved in the modelling strategy (stand age, CH, BA, and GSV) were characterized through the use of linear correlation analysis. The stand estimates of FC, BA, GSV, and CAI obtained from ALS data were assessed versus the respective inventory observations, summarizing the results by means of standard accuracy statistics (correlation coefficient, r; root mean square error, RMSE; and mean bias error, MBE).

## 3. Results

Figure 3 shows the spatial distribution of the umbrella pine stands within the San Rossore Park and the position of the 32 stands selected as described above. The main characteristics of the latter stands derived from the two SRFI inventories and interpolated in 2015 are provided by the summary statistics shown in Table 1. Their age varies between 30 and about 130 years, with an average close to 88 years; therefore, most of the plots are old-growth forests, and only three of them are relatively young (around 30 years). The CH average and standard deviation are 22.0 $\pm$ 2.6 m, with minimum and maximum values from 14 to 26 m. BA is high, i.e., 25.9 $\pm$ 5.5 $m^2$ $ha^{-1}$, with a range between 14 and 38 $m^2$ $ha^{-1}$. The observed GSV is 410 $\pm$ 85.1 $m^3$ $ha^{-1}$ and ranges between 222 and 583 $m^3$ $ha^{-1}$; CAI is 6.6 $\pm$ 2.9 $m^3$ $ha^{-1}$ $y^{-1}$, with minimum and maximum values of 3.1 and 15.8 $m^3$ $ha^{-1}$ $y^{-1}$, respectively.

The inter-dependency between these variables is expressed in terms of the correlation coefficients shown in Table 2. Age is a major determinant of CH due to its obvious positive effect on tree dimension; however, the dependence of CH on age is slightly asymptotical, as demonstrated by the 0.03 correlation increase brought about by the fitting of a logarithmic instead of a linear function. Instead, BA is negatively and moderately dependent on age, mostly due to a reduction in the number of plants per stand induced by thinning operations during forest aging. This pattern is attested to by the observations of the two available inventories, which indicate a strong reduction in the number of trees, particularly for the youngest stands (up to 70%). As expected, GSV is strongly correlated with BA but only marginally with the other stand attributes, partly due to the contrasting influence of age on CH and BA.

Concerning CAI, a direct relationship is evident with BA and, to a minor extent, with GSV. The relationship is, however, negative and highly significant with CH and stand age.

More specifically, the relationship between CAI and age is visible in Figure 4, which also shows a fitted power function equation capable of accounting for over 80% of the CAI variance. This figure confirms the mentioned expectation of a negative asymptotical dependency of CAI on age, which should theoretically be considered by estimating FC and NV from ALS data.

The GPP estimates obtained using Modified C-Fix for the entire park area, which are representative of total ecosystem production, are displayed in Figure 3. The GPP predicted for the umbrella pine stands ranges from 1500 to 1900 g C $m^{-2}$ $y^{-1}$, with an average around 1750 g C $m^{-2}$ $y^{-1}$. Similar estimates are obtained by the use of BIOME-BGC, which also simulates all other processes at equilibrium conditions. In particular, the autotrophic respiration predicted by this model accounts for about 68% of ecosystem GPP.

The CHM of the park area is displayed in Figure 5, with superimposed boundaries of the 32 selected umbrella pine stands. These stands are distributed within the whole umbrella pine forest strip, with the youngest stands placed in the south.

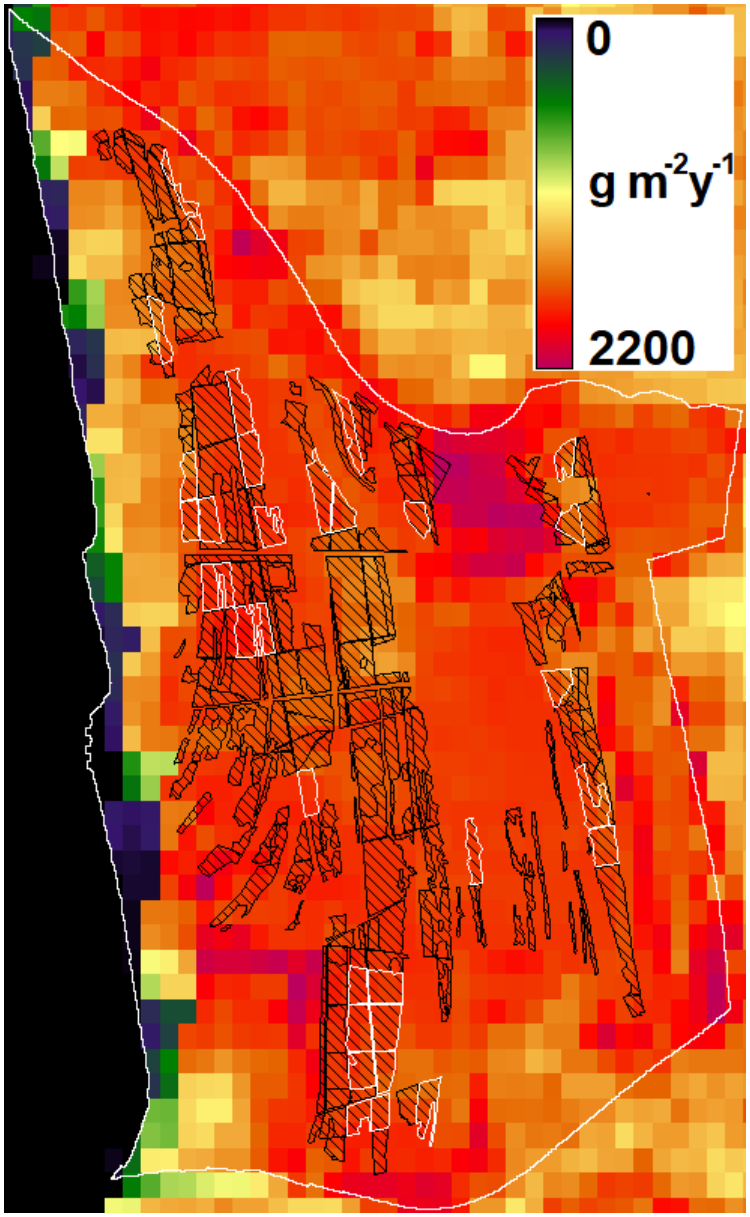


**Figure 3.** Mean GPP map obtained via Modified C-Fix for the years 2011–2015 with superimposed boundaries of the park (external white line) and stands covered by umbrella pines (black grid); the 32 stands bounded in white are those selected for statistical analysis.

**Table 1.** Summary statistics descriptive of the 32 forest stands considered derived from the inventory observations interpolated in 2015.

| Variable | Minimum | Maximum | Mean | Standard Deviation |
|---|---|---|---|---|
| Age (years) | 30 | 133 | 88 | 26.3 |
| CH (m) | 13.9 | 26.3 | 22.0 | 2.6 |
| BA ($m^2$ $ha^{-1}$) | 13.7 | 37.9 | 25.9 | 5.5 |
| GSV ($m^3$ $ha^{-1}$) | 222 | 583 | 410 | 85.1 |
| CAI ($m^3$ $ha^{-1}$ $y^{-1}$) | 3.1 | 15.8 | 6.6 | 2.9 |

**Table 2.** Correlations (r) found between observed age, CH, BA, GSV, and CAI (* = significant correlation, $p < 0.05$; ** = highly significant correlation, $p < 0.01$).

| r | CH | BA | GSV | CAI |
|---|---|---|---|---|
| Age | 0.868 ** | −0.215 | 0.293 | −0.831 ** |
| CH | | −0.412 * | 0.165 | −0.773 ** |
| BA | | | 0.828 ** | 0.542 ** |
| GSV | | | | 0.118 |

Figure 6 shows the scatter plots of the stand attributes observed and estimated through the use of ALS data. Among these, CH is slightly underestimated (r = 0.845, RMSE = 3.03 m and MBE = −2.71 m). The BA estimates, obtained from FC values ranging from 0.5 to 0.9 (average = 0.74), are less accurate in terms of variance explained but still satisfactory in terms of errors (r = 0.567, RMSE = 4.82 $m^2$ $ha^{-1}$ and MBE = 1.50 $m^2$ $ha^{-1}$). The combination of CH and BA yields GSV estimates that are only moderately accurate, i.e., r = 0.545, RMSE = 77.9 $m^3$ $ha^{-1}$ and MBE = −26.3 $m^3$ $ha^{-1}$ (Figure 6C).

The normalization of GSV into NV yields stand estimates that are mostly higher than 0.5 (average = 0.56). When combined with BIOME-BGC potential LAI values around 4, these estimates yield FC estimates that are much higher and less differentiated than those obtained when using the ALS data (from 0.8 to 0.95, average = 0.89). These patterns are obviously relevant for the prediction of NPP via Equation (2).

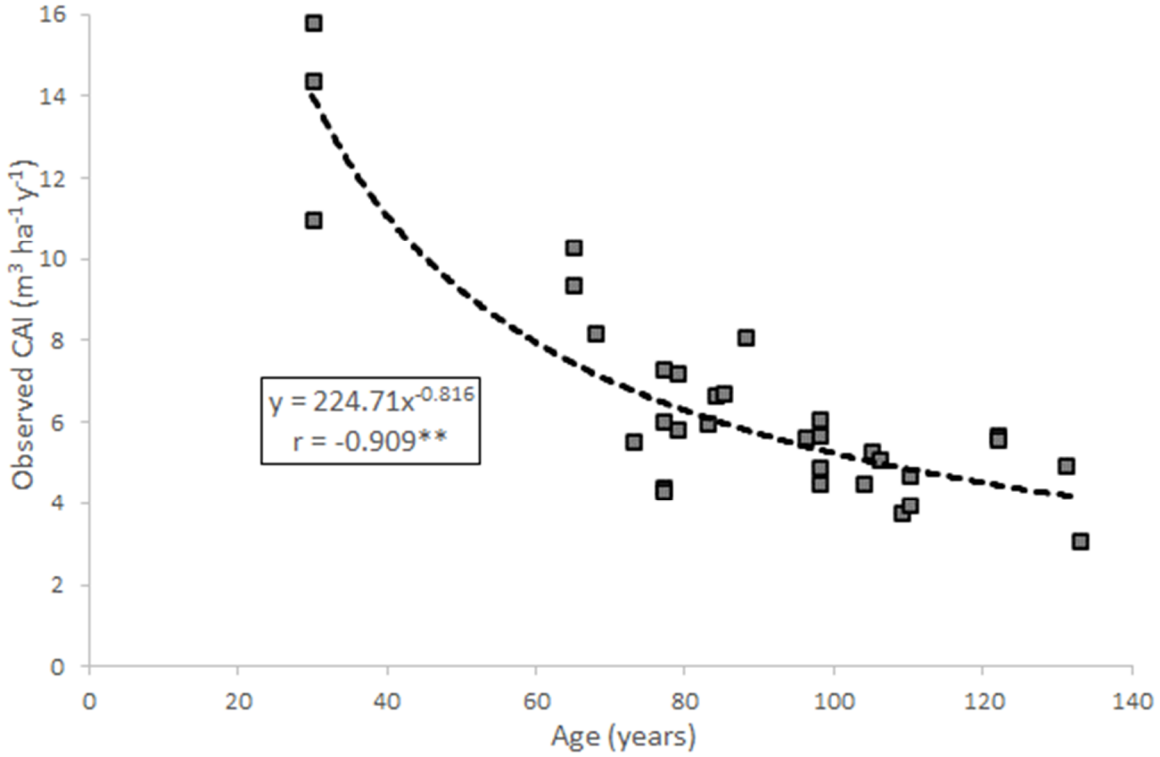


**Figure 4.** Dependency of CAI ($m^3$ $ha^{-1}$ $y^{-1}$) on forest age (years) as derived from the SRFI observations in the 32 pine stands considered (the line indicates the fitted exponential equation reported in the legend to which r is referred; ** = highly significant correlation, $p < 0.01$).

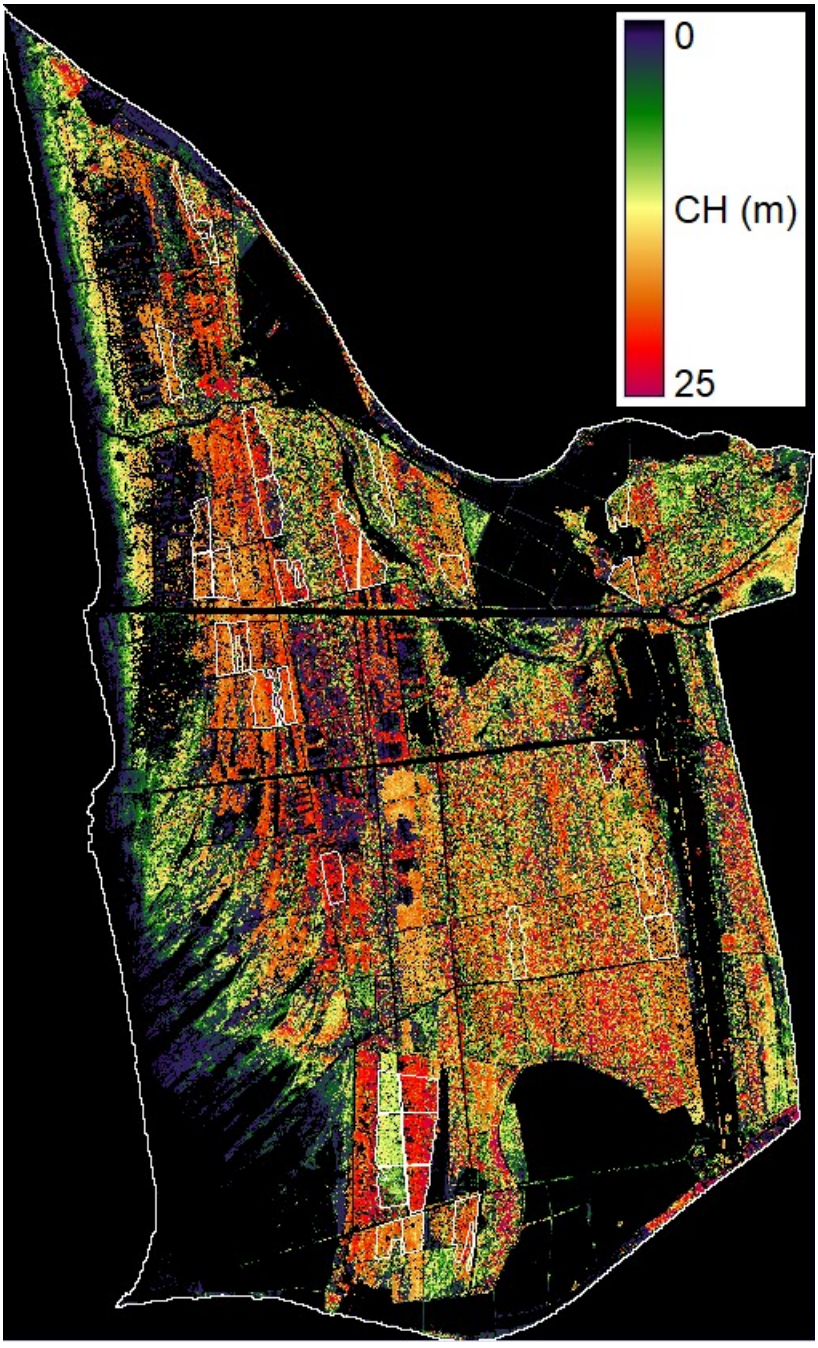


**Figure 5.** ALS CHM of May 2015 with with superimposed boundaries of the park area and of the 32 selected forest stands (while lines).

The conversion of GPP into NPP through this equation, in fact, yields stand estimates of around 830 g $m^{-2}$ $y^{-1}$, which correspond to a CAI of 8–9 $m^3$ $ha^{-1}$ $y^{-1}$. These estimates are plotted versus the respective stand ages in Figure 7, together with the fitted line of Figure 4. The CAI estimates show only a marginal tendency to follow this line, which indicates their poor dependence on age.

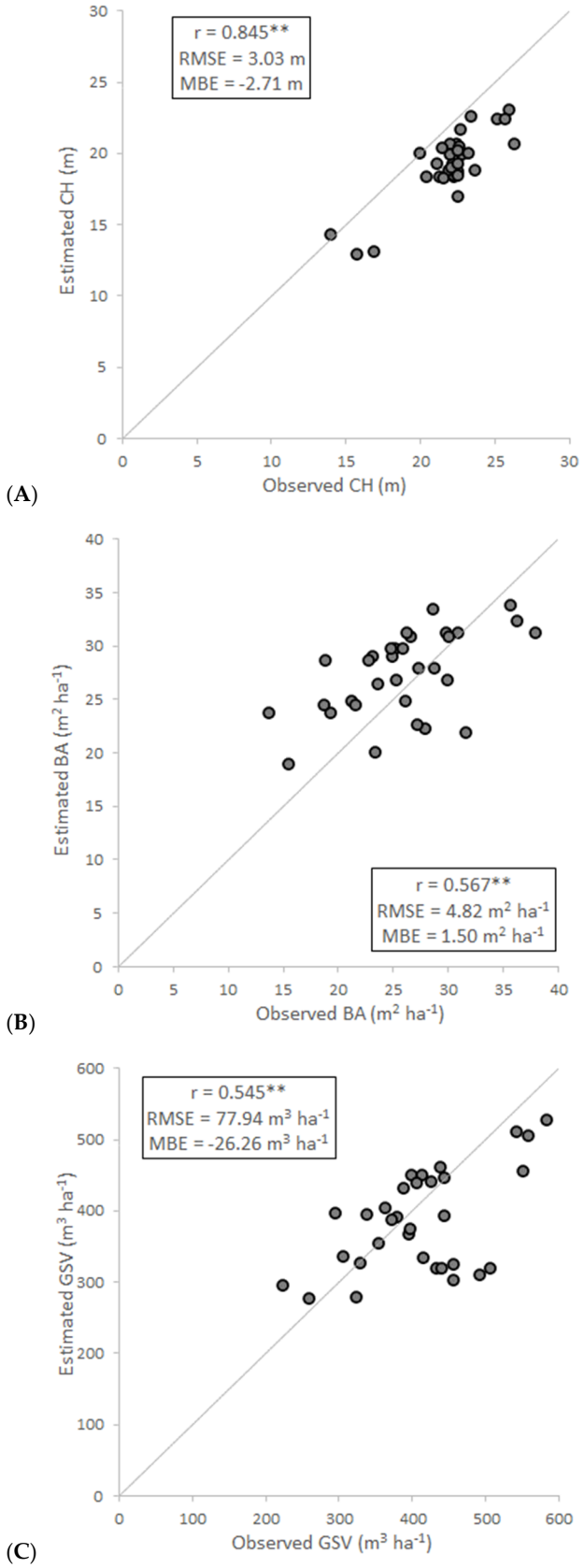


**Figure 6.** Comparison between the stand CH (**A**), BA (**B**), and GSV (**C**) values observed and estimated via the processing of the ALS CHM (** = highly significant correlation, $p < 0.01$).

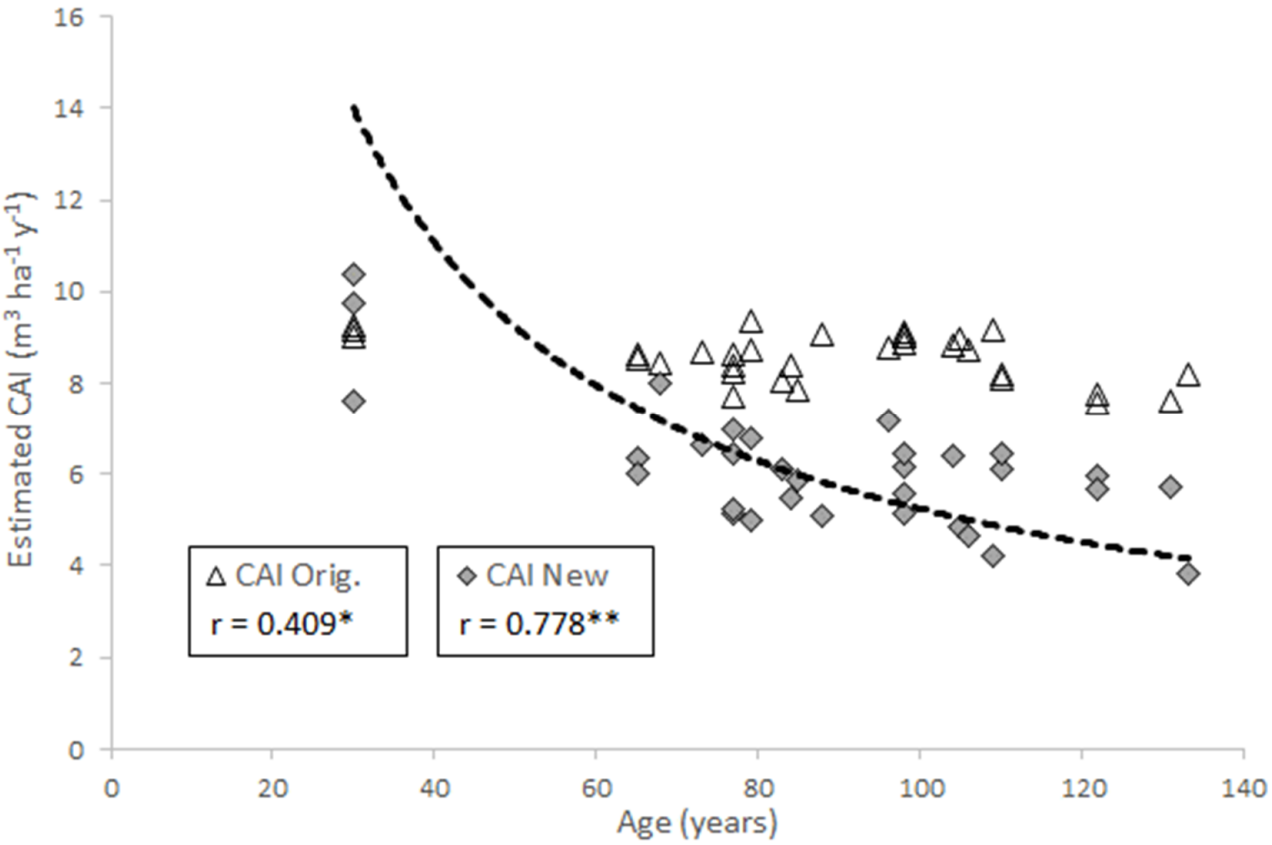


**Figure 7.** Age dependence of the stand CAI values estimated via the original and new modelling strategies. The correlation coefficients are calculated with respect to the dotted line, which is the same as in Figure 4 (* = significant correlation, $p < 0.05$; ** = highly significant correlation, $p < 0.01$).

On the contrary, driving Equation (2) with the lower and more differentiated ALS FC estimates yields CAI values that are more dependent on age, as indicated by a significant correlation with the fitted line (r = 0.778) (Figure 7).

The accuracies of the CAI estimates obtained using the two methods are, correspondingly, quite different. The estimates obtained through the use of the original method poorly reproduce the CAI measurements (r = 0.38), mostly due to an underestimation of the youngest stands and a marked overestimation for the others. These problems are notably alleviated when using the new method, which yields the estimates plotted versus the respective ground observations shown in Figure 8. These CAI estimates are in good agreement with the observations (r = 0.773, RMSE = 2.03 $m^3$ $ha^{-1}$ $y^{-1}$ and MBE = −0.45 $m^3$ $ha^{-1}$ $y^{-1}$), with only a certain underestimation remaining for the high CAI values of the most juvenile stands.

The spatial distribution of the stand CAI observations and estimates is displayed in Figure 9. A general agreement between the two maps can be noted, particularly concerning the low CAI values in the central part of the park as well as the highest CAI values in the most juvenile southern stands.

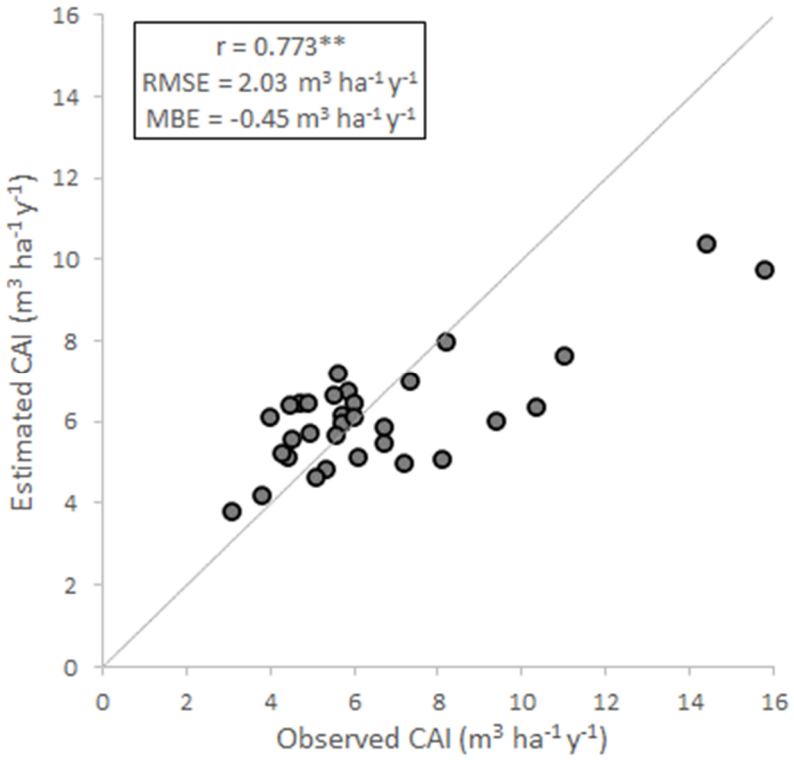


**Figure 8.** Comparison between stand CAI values observed and estimated via the described modelling strategy (** = highly significant correlation, $p < 0.01$).

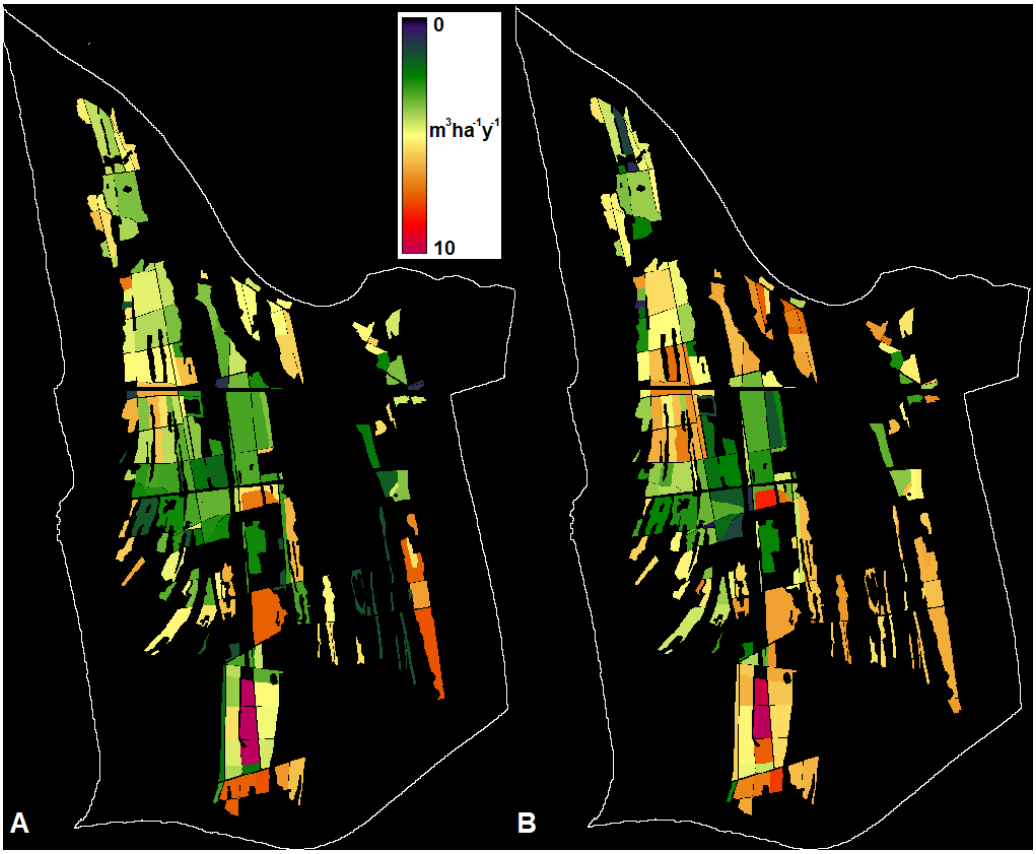


**Figure 9.** Maps of CAI observed (**A**) and estimated (**B**) in the umbrella pine stands fully characterized using both forest inventories.

## 4. Discussion

The original version of the current model combination strategy was developed and tested during investigations carried out both at local and regional scales (e.g., [18,22,24,29]). The strategy relies on sound scientific bases that guarantee the efficiency of the two models utilized and of the combination of their outputs.

Forest GPP is directly predicted by means of the parametric RUE model C-Fix adapted to Mediterranean environments, where plant growth is often limited by water stress during the dry period [37]. The accuracy of the C-Fix GPP estimates is obviously dependent on the quality of the meteorological and satellite imagery utilized [29,38]: both current datasets are available at a 250 m spatial resolution, which is acceptable in relatively homogeneous forest environments. The GPP estimates obtained are comparable to those observed at an eddy covariance flux tower that was installed in the same park within a different pine forest stand. The species monitored at that tower, in fact, was *Pinus pinaster* Ait. (Maritime pine), and the observation period was from 1999 to 2012 [39]; the mean annual GPP observed from 2001 to 2005 was around 1800 g C $m^{-2}$. Lower values were reported by flux tower observations taken in a Spanish Mediterranean pine wood ecosystem (about 1500 g C $m^{-2}$), and in the dry forest of Yatir, Israel (about 820 g C $m^{-2}$) [40].

In addition to C-Fix, this modelling strategy utilizes a version of the bio-geochemical model BIOME-BGC parameterized for Mediterranean pines. The model parameterization led to the identification of the evergreen needleleaf parameter settings reported in [32], which have been assessed in several cases for their capacity to reproduce both gross and net forest C fluxes [41].

The combination of C-Fix and BIOME-BGC outputs allows for the exploitation of the high efficiency of the RUE model in terms of estimating forest GPP and the capability of the bio-geochemical model to simulate all other ecosystem processes. As fully explained in [18], this combination strategy retains GSV as a crucial variable to characterize the actual status of the examined forests, which may be quite different from that considered through the use of BIOME-BGC. This model, in fact, simulates ecosystems in quasi-equilibrium with local environmental factors without taking into account the effects of human disturbances: the possible impacts of these are therefore incorporated using the ratio of actual over potential forest GSV (see Equation (2)).

The assessment of this model combination strategy has demonstrated its capacity to predict net forest C fluxes in areas where some fundamental assumptions used by BIOME-BGC can be considered reasonable [18,28]. This model, in fact, assumes the existence of a temporally stable ratio between photosynthetic and respiratory biomass pools, which corresponds to the presence of trees having diversified ages (development phases). In contrast, even-aged stands generally show a negative dependence of this ratio on age, which is due to several factors [21,22]. Among these, a major effect is exerted by the levelling off of photosynthetic tissues accompanied by the progressive accumulation of respiring woody biomass, which are both typical of homogeneously aging forests [42]. Forestry operations that are commonly applied to even-aged forest stands (tree cutting, thinning, etc.) can also alter the relationships among different biomass pools in a way that is difficult to assess over wide land areas and long time periods [43].

These problems can be overcome by estimating the existing forest biomass pools with high spatial resolution and accuracy, which can now be performed by relying on ALS datasets [44]. Numerous classical investigations, in fact, have shown the capability of these datasets to describe major forest attributes such as canopy density, BA and GSV [45]. Recently, [23] postulated that this capability could be exploited to characterize forest stands affected by different natural and human-induced factors and simulate the respective evolutions in terms of gross and net C fluxes.

These considerations are confirmed by the results of the current experiment, which concerns a sample of even-aged pine stands with different developmental stages. The statistical analysis carried out on this sample indicates that increasing stand age affects tree height positively while it has a minor and negative effect on the BA, which is likely

due to the thinning operations that are applied progressively during stand aging. As a consequence, the increase in GSV with age is marginal and likely associated with a slight decrease in canopy cover, which jointly induce a decrease in the difference between photosynthetic and respiratory tissues and, consequently, NPP and CAI. This pattern can also be explained by an eco-physiological explanation: aging trees become bigger in terms of stem radius and height but grow less rapidly due to increasing respiratory costs [42]. In most cases, this process is associated with a reduction in the number of standing trees due to forestry operations, particularly in the youngest stands [46].

Such patterns are poorly reproduced by the original modelling strategy, within which the stand GSV and canopy cover are linked through LAI. The reduction in the difference between photosynthesis and respiration simulated by this method, in fact, is entirely dependent on the increase in GSV, which, as previously noted, is only indirectly and approximately related to stand aging. Hence, the application of Equation (2) yields a poor dependence of CAI on age and a strong overestimation of CAI for the oldest stands. This issue is currently addressed via the separate estimation of the two scalars that regulate the functioning of Equation (2). These scalars are obtained via the processing of high-spatial-resolution ALS data, which allows for the modification of the relationship between simulated photosynthesis and respiration. This modification improves the capacity of the modelling strategy to take into account the effect of stand aging on both these processes. Consequently, the new method yields CAI estimates that are more strongly dependent on stand ages and are much more accurate.

The present findings agree with those of previous research on CAI estimation in similar environments as well as with eco-physiological considerations about C accumulation in differently managed stands. An example of the former case is provided by [20], who found that mature pine stands have a CAI dependence on age similar to that obtained here. Comparable results were obtained in studies performed in Italy at both regional and national levels by [24,47].

The transferability of the CAI simulation method to other forest areas is obviously dependent on the availability of high-spatial-resolution ALS datasets. Therefore, this operation is facilitated by national ALS data acquisition programs that have been completed or are currently in progress in several European countries [48]. The acquired datasets can be processed using both unsupervised and supervised techniques. In the former case, locally tuned allometric equations must preliminarily be defined, while in the latter case, the collection of statistically representative ground samples is usually required [49].

The various steps of the original NPP modelling method are affected by limitations and error sources, which have been analyzed and discussed in the mentioned papers [18,24]. A new issue introduced by the current modification concerns the estimation of FC in addition to GSV from the processing of ALS data. The current experimental results confirm the wide body of literature existing on this subject, indicating that moderate-to-good accuracy can be obtained through the use of unsupervised methods based on locally tuned allometric equations. This accuracy obviously affects that of the eventual CAI estimation, particularly for the youngest, most productive stands. The CAI underestimation currently found for these stands, in fact, is mostly derived from the approximate characterization of the respective FC and NV scalars. The modelling strategy would theoretically allow for the simulation of very high CAI values provided that these scalars are correctly estimated; for ex., in the case of a juvenile, extremely dense stand (CH = 3 m, FC = 0.9), the NPP/GPP ratio would approach 0.75, with a resulting CAI estimate of around 16 $m^3$ $ha^{-1}$ $y^{-1}$.

## 5. Conclusions and Future Prospects

This investigation is a natural extension of previous methodological studies aimed at simulating C fluxes and accumulation processes over wide forest areas. This study, in fact, focuses on an issue that is common in many managed forest stands, i.e., the impact of tree aging on C cycling and storage. In particular, this study has built on a consolidated

model combination strategy, demonstrating that it can be adapted to simulate the NPP of even-aged forest stands through the use of high-spatial-resolution ALS datasets.

The general validity of the current results is, of course, constrained by the limited size and specific characteristics of the ground and satellite datasets utilized. This particularly concerns the consideration of only one tree species, Mediterranean umbrella pine, in a unique study area. Thus, future research should be directed to the verification of the proposed simulation method in other case studies, i.e., in different zones and forest ecosystems. These studies could also consider the application of this method to smaller land surfaces, taking advantage of the high-spatial-resolution datasets that are being acquired by most recent satellite missions. For example, the use of NDVI images taken by the Sentinel-2 Multi Spectral Imager, which was launched in 2016, would allow for the estimation of forest GPP with a spatial resolution of 10 m, which is obviously relevant in terms of fragmented and heterogeneous areas.

**Author Contributions:** Conceptualization, F.M. and M.C.; methodology, M.C.; software, L.F.; validation, M.C. and L.F.; formal analysis, S.V.; investigation, G.C.; data curation, L.B. and L.F.; writing—original draft preparation, M.C. and F.M.; writing—review and editing, S.V. and G.C.; supervision, F.M. All authors have read and agreed to the published version of the manuscript.

**Funding:** This research received no external funding.

**Data Availability Statement:** The data cited in this manuscript are available in registries that are freely accessible to the public (https://modis.gsfc.nasa.gov, accessed on 8 January 2024).

**Acknowledgments:** The authors want to thank the San Rossore Natural Park in the person of F. Logli for providing access to the study area and the 2020 SRFI dataset.

**Conflicts of Interest:** The authors declare no conflicts of interest.

## Abbreviations

| | |
|---|---|
| ALS | Airborne laser scanning |
| BA | Basal area ($m^2$ $ha^{-1}$) |
| BEF | Biomass expansion factor |
| BWD | Basic wood density (mg $m^{-3}$) |
| C | carbon |
| CAI | Current annual increment ($m^3$ $ha^{-1}$ $year^{-1}$) |
| CH | Canopy height (m) |
| CHM | Canopy height model (m) |
| Cws | Water stress coefficient |
| fAPAR | Fraction of absorbed PAR |
| FC | Forest cover |
| GPP | Gross primary production (g C $m^{-2}$ $day^{-1}$) |
| GSV | Growing stock volume ($m^3$ $ha^{-1}$) |
| MODIS | Moderate Resolution Imaging Spectroradiometer |
| MVC | Maximum value composite |
| NDVI | Normalized difference vegetation index |
| NEP | Net ecosystem production (g C $m^{-2}$ $day^{-1}$) |
| NPP | Net primary production (g C $m^{-2}$ $day^{-1}$) |
| NS | Normalized sock |
| NV | Normalized volume |
| PAR | Photosynthetically active radiation (MJ $m^{-2}$) |
| PET | Potential evapotranspiration (mm $day^{-1}$) |
| Rgr | Growth respiration (g C $m^{-2}$ $day^{-1}$) |
| Rmn | Maintenance respiration (g C $m^{-2}$ $day^{-1}$) |
| RUE | Radiation use efficiency (g C $MJ^{-1}$ APAR) |
| SCA | Stem carbon allocation |
| SRFI | San Rossore forest inventory |

## References


1. Pan, Y.; Birdsey, R.A.; Fang, J.; Houghton, R.; Kauppi, P.E.; Kurz, W.A.; Phillips, O.L.; Shvidenko, A.; Lewis, S.L.; Canadell, J.G.; et al. A large and persistent carbon sink in the world's forests. *Science* **2011**, *333*, 988–993. [CrossRef] [PubMed]
2. Mo, L.; Zohner, C.M.; Reich, P.B.; Liang, J.; de Miguel, S.; Nabuurs, G.-J.; Renner, S.S.; Hoogen, J.v.D.; Araza, A.; Herold, M.; et al. Integrated global assessment of the natural forest carbon potential. *Nature* **2023**, *624*, 92–101. [CrossRef]
3. Bastin, J.-F.; Finegold, Y.; Garcia, C.; Mollicone, D.; Rezende, M.; Routh, D.; Zohner, C.M.; Crowther, T.W. The global tree restoration potential. *Science* **2019**, *365*, 75–79. [CrossRef] [PubMed]
4. Veldman, J.W.; Aleman, J.C.; Alvarado, S.T.; Anderson, T.M.; Archibald, S.; Bond, W.J.; Boutton, T.W.; Buchmann, N.; Buisson, E.; Canadell, J.G.; et al. Comment on "The global tree restoration potential". *Science* **2019**, *366*, 6463. [CrossRef]
5. Allard, V.; Ourcival, J.-M.; Rambal, S.; Joffre, R.; Rocheteau, A. Seasonal and annual variation of carbon exchange in an evergreen Mediterranean forest in southern France. *Glob. Chang. Biol.* **2008**, *14*, 714–725. [CrossRef]
6. Chapin, F.S., III; Woodwell, G.M.; Randerson, J.T.; Rastetter, E.B.; Lovett, G.M.; Baldocchi, D.D.; Clark, D.A.; Harmon, M.E.; Schimel, D.S.; Valentini, R.; et al. Reconciling carbon cycle concepts, terminology, and methods. *Ecosystems* **2006**, *9*, 1041–1050. [CrossRef]
7. Waring, R.H.; Running, S.W. *Forest Ecosystems: Analysis at Multiple Scales*, 3rd ed.; Academic Press: San Diego, CA, USA, 2007.
8. Rodeghiero, M.; Tonolli, S.; Vescovo, L.; Gianelle, D.; Cescatti, A.; Sottocornola, M. INFOCARB: A regional scale forest carbon inventory (Provincia Autonoma di Trento, Southern Italian Alps). *For. Ecol. Manag.* **2010**, *259*, 1093–1101. [CrossRef]
9. Levy, P.E.; Hale, S.E.; Nicoli, B.C. Biomass expansion factors and root: Shoot ratios for coniferous tree species in Great Britain. *Forestry* **2004**, *77*, 421–430. [CrossRef]
10. Federici, S.; Vitullo, M.; Tulipano, S.; De Lauretis, R.; Seufert, G. An approach to estimate carbon stocks change in forest carbon pools under the UNFCCC: The Italian case. *iForest* **2008**, *1*, 86–95. [CrossRef]
11. Clark, D.A.; Brown, S.; Kicklighter, D.W.; Chambers, J.Q.; Gower, S.T.; Thomlinson, J.; Ni, J. Measuring net primary production in forests: A synthesis of current concepts and field methods. *Ecol. Appl.* **2001**, *11*, 356–370. [CrossRef]
12. Fehrmann, L.; Kleinn, C. General considerations about the use of allometric equations for biomass estimation on the example of Norway spruce in central Europe. *For. Ecol. Manag.* **2006**, *236*, 412–421. [CrossRef]
13. Miehle, P.; Grote, R.; Battaglia, M.; Feikema, P.M.; Arndt, S.K. Evaluation of a process-based ecosystem model for long-term biomass and stand development of Eucalyptus globulus plantations. *Eur. J. For. Res.* **2010**, *129*, 377–391. [CrossRef]
14. Su, Y.; Zhang, W.; Liu, B.; Tian, X.; Chen, S.; Wang, H.; Mao, Y. Forest carbon flux simulation using multi-source data and incorporation of remotely sensed model with process-based model. *Remote Sens.* **2022**, *14*, 4766. [CrossRef]
15. Masek, J.G.; Collatz, G.J. Estimating forest carbon fluxes in a disturbed southeastern landscape: Integration of remote sensing, forest inventory, and biogeochemical modelling. *J. Geophys. Res.* **2006**, *111*, G01006. [CrossRef]
16. Yan, M.; Tian, X.; Li, Z.; Chen, E.; Wang, X.; Han, Z.; Sun, H. Simulation of forest carbon fluxes using model incorporation and data assimilation. *Remote Sens.* **2016**, *8*, 567. [CrossRef]
17. Zhao, J.; Lu, D.; Cao, Y.; Zhang, L.; Peng, H.; Wang, K.; Xi, H.; Wang, C. An integrated remote sensing and model approach for assessing forest carbon fluxes in China. *Sci. Total Environ.* **2022**, *811*, 152480. [CrossRef] [PubMed]
18. Maselli, F.; Chiesi, M.; Moriondo, M.; Fibbi, L.; Bindi, M.; Running, S.W. Modelling the forest carbon budget of a Mediterranean region through the integration of ground and satellite data. *Ecol. Model.* **2009**, *220*, 330–342. [CrossRef]
19. Bond-Lamberty, B.; Chuankuan, W.; Stith, T.G. Net primary production and net ecosystem production of a boreal black spruce wildfire chronosequence. *Glob. Chang. Biol.* **2004**, *10*, 473–487. [CrossRef]
20. Goulden, M.L.; Mcmillan, A.M.S.; Winston, G.C.; Rocha, A.V.; Manies, K.L.; Harden, J.W.; Bond-Lamberty, B.P. Patterns of NPP, GPP, respiration, and NEP during boreal forest succession. *Glob. Chang. Biol.* **2010**, *17*, 855–871. [CrossRef]
21. He, L.; Chen, J.M.; Pan, H.; Birdsey, R.; Kattge, J. Relationships between net primary productivity and forest stand age in U.S. forests. *Glob. Chang. Biol.* **2012**, *26*, GB3009. [CrossRef]
22. Chiesi, M.; Cherubini, P.; Maselli, F. Adaptation of a modelling strategy to predict the NPP of even-aged forest stands. *Eur. J. For. Res.* **2012**, *131*, 1175–1184. [CrossRef]
23. Chiesi, M.; Fibbi, L.; Vanucci, S.; Maselli, F. Use of remote sensing and biogeochemical modelling to simulate the impact of climatic and anthropogenic factors on forest carbon fluxes. *Remote Sens.* **2024**, *16*, 232. [CrossRef]
24. Chirici, G.; Chiesi, M.; Fibbi, L.; Giannetti, F.; Corona, P.; Maselli, F. High spatial resolution modelling of net forest carbon fluxes based on ground and remote sensing data. *Agric. For. Meteorol.* **2022**, *316*, 108866. [CrossRef]
25. DREAM. *Tenuta di San Rossore. Note Illustrative della Carta Forestale e della Fruizione Turistica*; S.E.L.C.A.: Firenze, Italy, 2003.
26. Thornton, P.E.; Running, S.W.; White, M.A. Generating surfaces of daily meteorological variables over large regions of complex terrain. *J. Hydrol.* **1997**, *190*, 214–251. [CrossRef]
27. Fibbi, L.; Maselli, F.; Pieri, M. Improved estimation of global solar radiation over rugged terrains by the disaggregation of Satellite Applications Facility on Land Surface Analysis data (LSA SAF). *Meteorol. Appl.* **2020**, *27*, e1940. [CrossRef]
28. Chirici, G.; Chiesi, M.; Corona, P.; Salvati, R.; Papale, D.; Fibbi, L.; Sirca, C.; Spano, D.; Duce, P.; Marras, S.; et al. Estimating daily forest carbon fluxes using a combination of ground and remotely sensed data. *J. Geophys. Res. Biogeosci.* **2016**, *121*, 266–279. [CrossRef]
29. Maselli, F.; Papale, D.; Puletti, N.; Chirici, G.; Corona, P. Combining remote sensing and ancillary data to monitor the gross productivity of water-limited forest ecosystems. *Remote Sens. Environ.* **2009**, *113*, 657–667. [CrossRef]

30. Running, S.W.; Zhao, M. User's Guide. Daily GPP and Annual NPP (MOD17A2H/A3H) and Year-End Gap-Filled (MOD17A2HGF/A3HGF) Products NASA Earth Observing System MODIS Land Algorithm (For Collection 6.1). Version 1.1. *Process. DAAC* **2021**.
31. Golinkoff, J. Biome BGC Version 4.2: Theoretical Framework of Biome-BGC. January 2010. Available online: http://www.ntsg.umt.edu/project/biome-bgc (accessed on 14 April 2014).
32. White, M.A.; Thornton, P.E.; Running, S.W.; Nemani, R.R. Parameterization and sensitivity analysis of the BIOME-BGC terrestrial ecosystem model: Net primary production controls. *Earth Interact.* **2000**, *4*, 1–85. [CrossRef]
33. Liu, S.; Bond-Lamberty, B.; Hicke, J.A.; Vargas, R.; Zhao, S.; Chen, J.; Edburg, S.L.; Hu, Y.; Liu, J.; McGuire, A.D.; et al. Simulating the impacts of disturbances on forest carbon cycling in North America: Processes, data, models, and challenges. *J. Geophys. Res. Biogeosci.* **2011**, *116*, G00K08. [CrossRef]
34. Schepaschenko, D.; Shvidenko, A.; Usoltsev, V.; Lakyda, P.; Luo, Y.; Vasylyshyn, R.; Lakyda, I.; Myklush, Y.; See, L.; McCallum, I.; et al. A dataset of forest biomass structure for Eurasia. *Sci. Data* **2017**, *4*, 170070. [CrossRef]
35. Næsset, E. Predicting forest stand characteristics with airborne scanning laser using a practical two-stage procedure and field data. *Remote Sens. Environ.* **2002**, *80*, 88–99. [CrossRef]
36. Maselli, F.; Mari, R.; Chiesi, M. Use of LiDAR data to simulate forest net primary production. *Int. J. Remote Sens.* **2013**, *34*, 2487–2501. [CrossRef]
37. Sardans, J.; Peñuelas, J. Plant-soil interactions in Mediterranean forest and shrublands: Impacts of climatic change. *Plant Soil* **2013**, *365*, 1–33. [CrossRef] [PubMed]
38. Gilabert, M.A.; Moreno, A.; Maselli, F.; Martínez, B.; Chiesi, M.; Sánchez, S.; García-Haro, F.J.; Carrara, A.; Pérez-Priego, O.; Serrano, P. Daily GPP estimates in Mediterranean ecosystems combining remote sensing and meteorological data. *ISPRS J. Photogramm. Remote Sens.* **2015**, *102*, 184–197. [CrossRef]
39. Pastorello, G.; Trotta, C.; Canfora, E.; Chu, H.; Christianson, D.; Cheah, Y.-W.; Poindexter, C.; Chen, J.; Elbashandy, A.; Humphrey, M.; et al. The FLUXNET2015 dataset and the ONEFlux processing pipeline for eddy covariance data. *Sci Data* **2020**, *7*, 225. [CrossRef] [PubMed]
40. Rotenberg, E.; Yakir, D. Contribution of semi-arid forests to the climate system. *Science* **2010**, *237*, 451–454. [CrossRef]
41. Chiesi, M.; Fibbi, L.; Genesio, L.; Gioli, B.; Magno, R.; Maselli, F.; Moriondo, M.; Vaccari, F. Integration of ground and satellite data to model Mediterranean forest processes. *Int. J. Appl. Earth Obs. Geoinf.* **2011**, *13*, 504–515. [CrossRef]
42. West, P.W. Do increasing respiratory costs explain the decline with age of forest growth rate? *J. For. Res.* **2020**, *31*, 693–712. [CrossRef]
43. Nolet, P.; Kneeshaw, D.; Messier, C.; Béland, M. Comparing the effects of even- and uneven- aged silviculture on ecological diversity and processes: A review. *Ecol. Evol.* **2018**, *8*, 1217–1226. [CrossRef]
44. Zhao, K.; Suarez, J.C.; Garcia, M.; Hu, T.; Wang, C.; Londob, A. Utility of multitemporal lidar for forest and carbon monitoring: Tree growth, biomass dynamics, and carbon flux. *Remote Sens. Environ.* **2018**, *204*, 883–897. [CrossRef]
45. Coops, N.; Tompalski, P.; Goodbody, T.R.H.; Queinnec, M.; Luther, J.E.; Bolton, D.K.; White, J.C.; Wulder, M.A.; van Lier, O.R.; Hermosilla, T. Modelling lidar-derived estimates of forest attributes over space and time: A review of approaches and future trends. *Remote Sens. Environ.* **2021**, *260*, 112477. [CrossRef]
46. Hynynen, J.; Eerikäinen, K.; Mäkinen, H.; Valkonen, S. Growth response to cuttings in Norway spruce stands under even-aged and uneven-aged management. *For. Ecol. Manag.* **2019**, *437*, 314–323. [CrossRef]
47. Chirici, G.; Chiesi, M.; Corona, P.; Puletti, N.; Mura, M.; Maselli, F. Prediction of forest NPP in Italy by the combination of ground and remote sensing data. *Eur. J. For. Res.* **2015**, *134*, 453–467. [CrossRef]
48. Stoker, J.M.; Harding, D.; Parrish, J. The need for a national LIDAR dataset. *Photogramm. Eng. Remote Sens.* **2008**, *74*, 1066–1068.
49. Wulder, M.A.; Bater, C.W.; Coops, N.C.; Hilker, T.; White, J.C. The role of LiDAR in sustainable forest management. *For. Chron.* **2008**, *84*, 807–826. [CrossRef]